JACS
JOURNAL OF THE AMERICAN CHEMICAL SOCIETY
Article
pubs.acs.org/JACS

High Thermoelectric Performance Realized in a BiCuSeO System by Improving Carrier Mobility through 3D Modulation Doping

Yan-Ling Pei,*[,†,#] Haijun Wu,[‡,#] Di Wu,[‡] Fengshan Zheng,[‡] and Jiaqing He*[,‡]

[†]School of Materials Science and Engineering, Beihang University, Beijing 100191, China
[‡]Department of Physics, South University of Science and Technology of China, Shenzhen 518055, China

Supporting Information

ABSTRACT: We report a greatly enhanced thermoelectric performance in a BiCuSeO system, realized by improving carrier mobility through modulation doping. The heterostructures of the modulation doped sample make charge carriers transport preferentially in the low carrier concentration area, which increases carrier mobility by a factor of 2 while maintaining the carrier concentration similar to that in the uniformly doped sample. The improved electrical conductivity and retained Seebeck coefficient synergistically lead to a broad, high power factor ranging from 5 to 10 μW cm^{-1} K^{-2}. Coupling the extraordinarily high power factor with the extremely low thermal conductivity of ~0.25 W m^{-1} K^{-1} at 923 K, a high $ZT \approx 1.4$ is achieved in a BiCuSeO system.

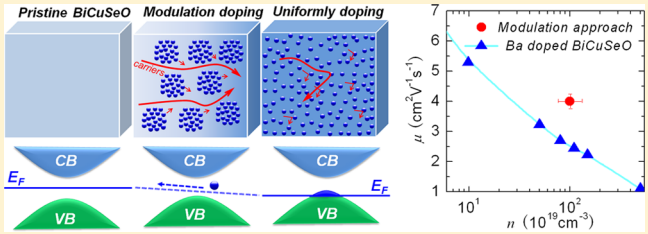

INTRODUCTION

Thermoelectric materials, which are capable of converting waste heat into electrical power and *vice versa*, are currently receiving significant scientific attention. The efficiency of a thermoelectric device is determined by the dimensionless figure of merit ZT. Conceptually, to ensure a high $ZT = (S^2\sigma/\kappa)T$, where S, σ, κ, and T are the Seebeck coefficient, the electrical conductivity, the thermal conductivity, and the absolute temperature in Kelvin, respectively, S and σ must both be large, while κ must be minimized so that the temperature difference can be maintained.[1] The laws of physics conspire against satisfying this requirement, because the Wiedemann–Franz law requires κ to be proportional to σ and the Pisarenko relation limits the value of $S^2\sigma$, which is the quantity that needs to be maximized.[2,3] Several approaches to enhance ZT have emerged in the past decades, including band structure engineering to enhance Seebeck coefficients,[4,5] nanostructuring and all-scale hierarchical architecturing to reduce thermal conductivity,[6,7] and band alignment to maintain hole mobility.[8] Most of these approaches aim to gain a high power factor while obtain a low lattice thermal conductivity. Alternatively, one can also seek high thermoelectric performance in pristine materials with intrinsically low thermal conductivity.[9−11]

Thermoelectric oxides comprise a promising branch of the overall thermoelectric materials, considering their potential advantages over heavy-metal alloys in terms of chemical and thermal robustness. The well-studied thermoelectric oxides, including $SrTiO_3$-,[12] $NaCoO_3$-,[13] $Ca_3Co_4O_9$-,[14] $CaMnO_3$-,[15] and In_2O_3-based[16] oxides, exhibit ZT values relatively lower than those of heavy-metal alloys, which can be ascribed to either moderate electrical conductivity or high thermal conductivity, depending on the families. Recently, we reported a quaternary oxyselenide system, BiCuSeO, as a promising thermoelectric material, and the ZT value of this oxide largely outperforms the others.[17] The intrinsically low thermal conductivity of BiCuSeO indicates that a practical way to enhance ZT is to increase its electrical transport properties, which are determined by both carrier concentration and carrier mobility.[18] Indeed, the ZT has already been improved by increasing carrier concentration to as high as ~1×10^{21} cm^{-3} through optimization of various dopants.[19−23] However, the relatively low carrier mobility (as low as ~22 cm^2 V^{-1} s^{-1}, even for pristine BiCuSeO) still greatly limits the ability to improve the electrical transport properties. Worse still, the carrier mobility is deteriorated to 1−2 cm^2 V^{-1} s^{-1} because of carriers scattering after doping with heavy elements. There is promising in the fact that a factor of 2 increase in carrier mobility was obtained by microstructure texturing through several hot-forging steps. This strategy thus proved to be an effective way to further enhance ZT from 1.1 to 1.4, taking advantage of the anisotropic nature of BiCuSeO.[24]

Modulation doping (MD) is a well-developed technique that is widely used in two-dimensional electron gas (2DEG) thin-film devices in order to improve the carrier mobility and thus the electrical conductivity.[25] A MD device normally consists of a doped layer, which provides charge carriers, and an undoped layer, which serves as the charge transport channel, free of parent impurity atoms. A typical example is the MgZnO/ZnO heterostructure. A super-high carrier mobility of 180 000 cm^2 V^{-1} s^{-1}, i.e., 9 times larger than that of the best synthetic ZnO defect-free single crystal, was reported in the MgZnO/ZnO heterostructures of 2DEG grown by molecular beam epitaxy (MBE).[26] Usually, doping is an effective way to enhance the

Received: August 3, 2014
Published: September 19, 2014

   dx.doi.org/10.1021/ja507945h | J. Am. Chem. Soc. 2014, 136, 13902−13908

electrical conductivity via increasing the carrier concentration; however, high-level dopants themselves can severely limit the carrier mobility and even cause the mobility to plummet. In the case of MgZnO/ZnO heterostructures, the electrons are generated in the MgZnO doped layers but transferred to ZnO undoped layers, which effectively avoids the scattering of the ionized defects in the ZnO layers. For several decades, the MD approach has been limited to 2D film structures, while MD of three-dimensional (3D) bulk structures remains unexplored. Recently, enhanced power factors were achieved in $Si_{1-x}Ge_x$ composites via constructing heterostructures consisting of one doped component and another undoped component.[27,28] The carrier mobility and power factor were found to be significantly enhanced, and the underlying mechanism was attributed to MD approach, the same as that in the 2D thin-film structures. All the above reports prompted us to investigate the scientific underpinning of these intriguing results and motivated us to apply the MD approach in a BiCuSeO system with intrinsically low thermal conductivity, in which the thermoelectric performance can probably be significantly enhanced by improving the carrier mobility and thus the electrical conductivity.

In this article, we introduce the concept of MD in 3D bulk materials to increase the thermoelectric figure of merit ZT in a BiCuSeO system. Since the heavy-hole $Bi_{0.875}Ba_{0.125}CuSeO$ sample exhibits the highest ZT = 1.1 at 923 K among BiCuSeO systems with an optimized carrier concentration,[21] in the present work it is expected that a higher ZT for $Bi_{0.875}Ba_{0.125}CuSeO$ could be obtained by additionally improving the carrier mobility. Our results show that the MD approach indeed boosts the carrier mobility by a factor of 2 without deteriorating the carrier concentration. The improved electrical conductivity, along with the nearly unchanged Seebeck coefficient, then leads to a broad, high power factor ranging from 5 to 10 μW cm^{-1} K^{-2}, which coupling with the low thermal conductivity of ∼0.25 W m^{-1} K^{-1} eventually results in a high $ZT \approx 1.4$ at 923 K in the BiCuSeO system. The present results indicate that the BiCuSeO system is a robust candidate for medium-temperature thermoelectric applications and point out that MD is indeed an effective approach to improve the carrier mobility in 3D bulks, just as it is in 2DEG thin-film structures.

EXPERIMENTAL SECTION

Synthesis. Uniformly Ba-doped samples with the chemical composition $Bi_{1-x}Ba_xCuSeO$ (x = 0, 0.125, and 0.25) were synthesized by a two-step solid-state reaction route. A stoichiometric mixture of Bi_2O_3 (4N), Bi (3N), Cu (3N), Se (5N), and BaO (3N) powders was mixed by a ball-milling process, and then the mixed powders were put into a graphite die, where they underwent cold pressing and heating at 573 K for 8 h and 1023 K for 24 h in a vacuum in a hot-pressing sinter. The obtained bulks were crushed into powders and then ball-milled at 250 rpm for 8 h in a planetary ball mill. Finally, the obtained powders were sintered by spark plasma sintering (SPS 1050, Sumimoto, Japan) under an axial compressive stress of 50 MPa in a vacuum at 973 K for 6 min, resulting in a disk-shaped sample of 20 mm × 7 mm. For the modulation, Ba-doped samples with the chemical composition of $Bi_{0.875}Ba_{0.125}CuSeO$ were prepared by mixing pristine BiCuSeO and $Bi_{0.75}Ba_{0.25}CuSeO$ powders at a mole ratio of 1:1 for 10 min via ball-milling, followed by the same SPS process as described above. All the sample preparation processes, including weighing raw materials and ball-milling, were carried out in air.

Electrical Transport Properties. The obtained SPS-processed pellets were cut along the radial direction of the disk-shaped sample into bars with dimensions of about 18 mm × 3 mm × 3 mm, which were then used for simultaneous measurements of the Seebeck coefficient and the electrical conductivity using a ZEM-2 instrument (Ulvac Riko, Japan) under a helium atmosphere from room temperature to 923 K. Heating and cooling cycles gave repeatable electrical properties to verify the thermal stability. Electrical properties obtained from different slices cut from the same pellets were similar, attesting to the homogeneity of the samples. The uncertainty of both the Seebeck coefficient and electrical conductivity measurements is 5%. The Hall coefficients (R_H) of the samples were measured at room temperature using a physical properties measurement system (PPMS-9T, Quantum Design Inc., USA), with an applied magnetic field of 2 T and electrical current of 30 mA. The carrier concentration (n_H) was calculated by using $n_H = 1/eR_H$, where e is the electronic charge. The carrier mobility (μ) was calculated by using $\mu = \sigma R_H$, where σ is the electrical conductivity. The uncertainty of the Hall measurement is also 5%.

Thermal Conductivity. High-density SPS-processed pellets were cut along the SPS pressing direction, and the thermal and electrical transport properties were measured along the same direction in the sample. The SPS-processed pellets were polished into rectangular samples with side lengths of 6 mm and ∼2 mm thickness for thermal diffusivity measurements. The samples were coated with a thin layer of graphite to minimize errors from the emissivity of the material. The thermal conductivity was calculated from $\kappa = DC_p\rho$, where the thermal diffusivity coefficient D in the range from room temperature to 923 K was measured using the laser flash diffusivity method (LFA 427, Netzsch, Germany). The thermal diffusivity data were analyzed using a Cowan model with pulse correction, and heating and cooling cycles gave reproducible values for each sample. The specific heat capacity (C_p) was determined by differential scanning calorimetry (DSC 404C, Netzsch, Germany). The density (ρ) was determined by using the dimensions and mass of the sample, and then reconfirmed using the Archimedes method. Thermal diffusivities obtained for different slices from the same pellet were also similar. The uncertainty of the thermal conductivity is estimated to be within 8%, considering the uncertainties for D, C_p, and ρ. The combined uncertainty for all measurements involved in the calculation of ZT is less than 15%.

X-ray Diffraction and Transmission Electron Microscopy. Samples were pulverized in an agate mortar for powder X-ray diffraction (XRD) studies. The XRD pattern was obtained with Cu Kα (λ = 1.54178 Å) radiation in a reflection geometry on an Inel diffractometer operating at 40 kV and 20 mA and equipped with a position-sensitive detector. Transmission electron microscopy (TEM) investigations were carried out on a JEOL 2100F microscope. The thin TEM specimens were prepared by conventional standard methods. The procedures include cutting, grinding, dimpling, polishing, and subsequently Ar-ion milling on a liquid nitrogen cooling stage.

RESULTS AND DISCUSSION

The overall operating concept that is the key to the generic design of MD is shown in Figure 1. The modulation doped sample is actually a two-phase composite, i.e., undoped BiCuSeO and heavily doped $Bi_{0.75}Ba_{0.25}CuSeO$. The pristine BiCuSeO shows a lower carrier concentration but higher carrier mobility, while heavily doped $Bi_{0.75}Ba_{0.25}CuSeO$ exhibits a higher carrier concentration but lower carrier mobility. The Fermi level of pristine BiCuSeO locates at the middle between the conduction and valence bands, and would move into the valence band in the case of heavily doped $Bi_{0.75}Ba_{0.25}CuSeO$. As for the modulation doped sample, $Bi_{0.875}Ba_{0.125}CuSeO$ (50% BiCuSeO + 50% $Bi_{0.75}Ba_{0.25}CuSeO$), the Fermi level is supposed to bridge the ones of the two end members. The Fermi level imbalance prompts the electrons diffuse from doped phase to undoped phase, where carrier mobility is higher owing to the less ionized scattering centers, thus resulting in an overall enhanced carrier mobility in comparison to uniformly doping.

dx.doi.org/10.1021/ja507945h | J. Am. Chem. Soc. 2014, 136, 13902−13908

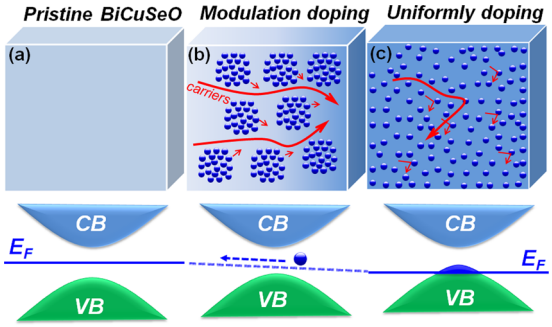

Figure 1. Three-dimensional schematic showing the band structures and Fermi energy levels for the pristine BiCuSeO, modulation doped $Bi_{0.875}Ba_{0.125}CuSeO$ (50% BiCuSeO + 50% $Bi_{0.75}Ba_{0.25}CuSeO$), and uniformly doped $Bi_{0.875}Ba_{0.125}CuSeO$. For the modulation doped sample, the carriers transport preferentially in the low carrier concentration area. The modulation approach shows similar carrier concentration but higher carrier mobility compared to the uniform one.

To systematically investigate the MD approach, several samples were prepared, including pristine BiCuSeO, uniformly doped $Bi_{0.875}Ba_{0.125}CuSeO$, modulation doped $Bi_{0.875}Ba_{0.125}CuSeO$ (50% BiCuSeO + 50% $Bi_{0.75}Ba_{0.25}CuSeO$), and heavily doped $Bi_{0.75}Ba_{0.25}CuSeO$. Figure 2 shows the

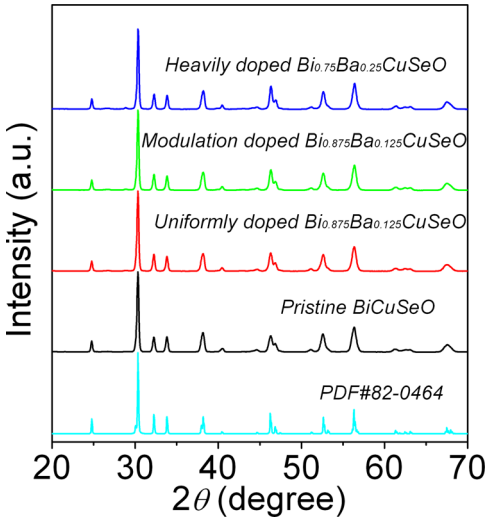

Figure 2. Powder XRD patterns for the pristine BiCuSeO, uniformly doped $Bi_{0.875}Ba_{0.125}CuSeO$, modulation doped $Bi_{0.875}Ba_{0.125}CuSeO$, and heavily doped $Bi_{0.75}Ba_{0.25}CuSeO$ samples.

powder XRD patterns for these four samples. All the Bragg peaks show an excellent match to the ones simulated for BiCuSeO (PDF No. 82-0464) and can be indexed as the ZrSiCuAs-type structure.

Figure 3a plots the room-temperature carrier mobility as a function of carrier concentration for the Ba-doped BiCuSeO, as well as the modulation doped one. All the Ba-doped samples follow a smooth curve that demonstrates an inversely proportional relationship between carrier mobility and carrier concentration. However, the carrier mobility of the modulation doped sample deviates from the curve and shows a significant enhancement. As shown in Figure 3b, the room-temperature carrier concentration is $\sim 1.1 \times 10^{18}$ cm^{-3} for pristine BiCuSeO. It then increases to $\sim 1.2 \times 10^{21}$ cm^{-3} for the uniformly doped $Bi_{0.875}Ba_{0.125}CuSeO$, and further increases to $\sim 5.0 \times 10^{21}$ cm^{-3}

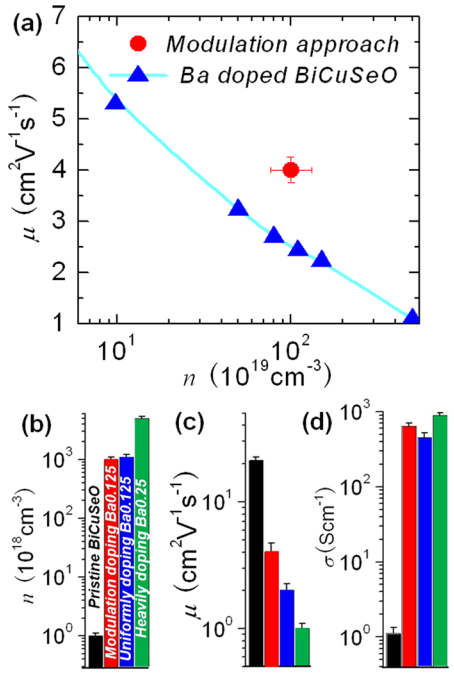

Figure 3. (a) Room-temperature carrier mobility as a function of carrier concentration for the uniformly doped $Bi_{1-x}Ba_xCuSeO$ and modulation doped $Bi_{0.875}Ba_{0.125}CuSeO$. Room temperature (b) carrier concentration, (c) carrier mobility, and (d) electrical conductivity for the pristine BiCuSeO (black), modulation doped $Bi_{0.875}Ba_{0.125}CuSeO$ (red), uniformly doped $Bi_{0.875}Ba_{0.125}CuSeO$ (blue), and heavily doped $Bi_{0.875}Ba_{0.125}CuSeO$ (green). The modulation doped $Bi_{0.875}Ba_{0.125}CuSeO$ shows a higher carrier mobility than the uniformly doped $Bi_{0.875}Ba_{0.125}CuSeO$ with a similar carrier concentration.

for the heavily doped $Bi_{0.75}Ba_{0.25}CuSeO$. The modulation doped $Bi_{0.875}Ba_{0.125}CuSeO$ shows a carrier concentration of $\sim 1.0 \times 10^{21}$ cm^{-3}, which is comparable to that of the uniformly doped $Bi_{0.875}Ba_{0.125}CuSeO$.[21] Figure 3c shows that the room-temperature carrier mobility is ~ 22 cm^2 V^{-1} s^{-1} for pristine BiCuSeO, which then decreases dramatically to ~ 2.1 cm^2 V^{-1} s^{-1} for the uniformly doped $Bi_{0.875}Ba_{0.125}CuSeO$ and ~ 1.0 cm^2 V^{-1} s^{-1} for the heavily doped $Bi_{0.75}Ba_{0.25}CuSeO$. The significant reduction in carrier mobility after Ba doping indicates a strong scattering of carriers. It is worth noting that the modulation doped $Bi_{0.875}Ba_{0.125}CuSeO$ shows a carrier mobility ~ 4.1 cm^2 V^{-1} s^{-1}, which is almost twice as high as that of the uniformly doped $Bi_{0.875}Ba_{0.125}CuSeO$ with a similar carrier concentration. This combination of carrier concentration and carrier mobility promotes a significant increase in the room-temperature electrical conductivity from 454 S cm^{-1} for the uniformly doped $Bi_{0.875}Ba_{0.125}CuSeO$ to 640 S cm^{-1} for the modulation doped $Bi_{0.875}Ba_{0.125}CuSeO$ (Figure 3d). These results experimentally confirm the idea proposed in Figure 1.

The effects of MD on the thermoelectric transport properties can be seen in Figure 4, where the temperature dependence of the thermoelectric properties for the pristine BiCuSeO, modulation doped $Bi_{0.875}Ba_{0.125}CuSeO$, uniformly doped $Bi_{0.875}Ba_{0.125}CuSeO$, and heavily doped $Bi_{0.75}Ba_{0.25}CuSeO$ are compared. Upon Ba doping (Figure 4a), the electrical transport changes to a metallic-like behavior and shows a systematic enhancement with the increase of Ba doping, from ~ 1.12 S cm^{-1} for BiCuSeO to ~ 888 S cm^{-1} for $Bi_{0.75}Ba_{0.25}CuSeO$ at 300 K, which is consistent with the strongly increased carrier concentration. Notably, the modulation doped

dx.doi.org/10.1021/ja507945h | J. Am. Chem. Soc. 2014, 136, 13902−13908

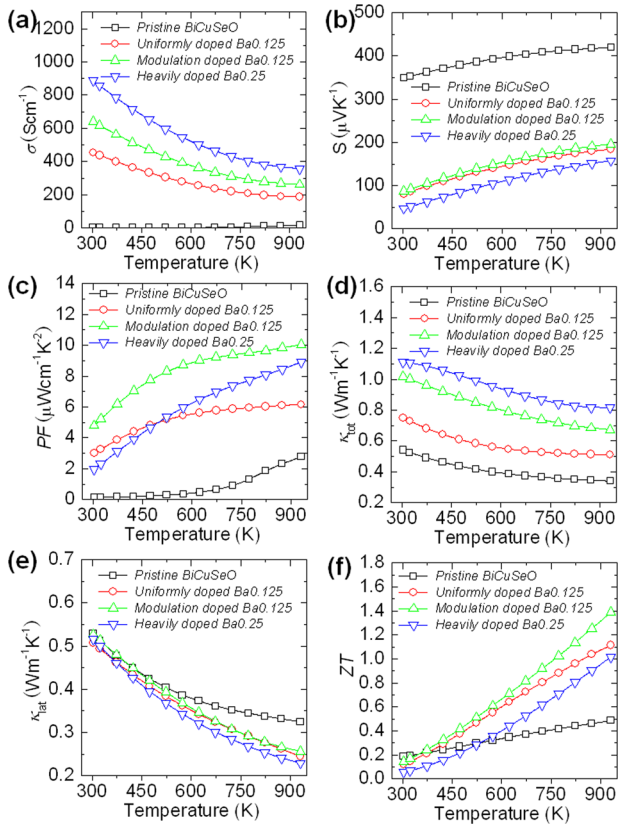

Figure 4. Thermoelectric properties as a function of temperature for the pristine BiCuSeO, modulation doped $Bi_{0.875}Ba_{0.125}CuSeO$, uniformly doped $Bi_{0.875}Ba_{0.125}CuSeO$, and heavily doped $Bi_{0.75}Ba_{0.25}CuSeO$: (a) electrical conductivity, (b) Seebeck coefficient, (c) power factor, (d) total thermal conductivity, (e) lattice thermal conductivity, and (f) figure of merit ZT. The combined uncertainty for all measurements involved in the calculation of ZT is less than 15%.

$Bi_{0.875}Ba_{0.125}CuSeO$ shows a much higher electrical conductivity in the entire measurement temperature range than the uniformly doped $Bi_{0.875}Ba_{0.125}CuSeO$,[21] due to the improvement in carrier mobility, since their carrier concentrations are comparable.

To quantitatively evaluate the effect of the MD on enhancing the electrical conductivity, we calculate the effective electrical conductivity on the basis of self-consistent effective medium theory (EMT).[29] The effective electrical conductivity (σ_{eff}) value of a heterogeneous composite consisting of undoped (σ_1) and doped (σ_2) regions should satisfy the following expression:

$$f_1\frac{\sigma_1-\sigma_{eff}}{\sigma_1+2\sigma_{eff}}+f_2\frac{\sigma_2-\sigma_{eff}}{\sigma_2+2\sigma_{eff}}=0 \quad (1)$$

where f_1 and f_2 are the volume fractions of the undoped and doped regions ($f_1 = f_2 = 0.5$ in this case), $\sigma_1 = en_1\mu_1$, and $\sigma_2 = en_2\mu_2$. Here, the carrier concentrations n_1 and n_2, and the carrier mobilities μ_1 and μ_2, are the respective ones in the pristine and heavily doped terminals. Without considering carrier redistribution, $n_1 = 1.0 \times 10^{18}$ cm^{-3} and $n_2 = 5.0 \times 10^{21}$ cm^{-3} for pristine and heavily doped BiCuSeO, individually; the σ_{eff} is then estimated to be only 260 S cm^{-1}, which is far away from the experimental value (640 S cm^{-1}). The significant discrepancy requires some explanation other than simply combining two independent phases; charge transfer and redistribution are thus proposed.

The charge carrier redistribution between pristine and doped grains was estimated through solving the Poisson equation self-consistently[30] (the details can be found in the Supporting Information (SI)). To begin with, the Fermi level difference (before contact) between the two kinds of adjacent grains needs to be estimated on the basis of the following relationships:[31]

$$n(\eta)=4\pi\left(\frac{2m^*k_BT}{h^2}\right)^{3/2}\frac{F_{1/2}(\eta)}{r_H} \quad (2)$$

$$F_{1/2}(\eta)=\int_0^\infty\frac{x^{1/2}}{1+e^{x-\eta}}dx \quad (3)$$

$$\eta=\frac{E_F}{k_BT} \quad (4)$$

where m^* is the effective mass, h the Planck constant, $F_{1/2}(\eta)$ the half-order Fermi integral in the case of acoustic phonon scattering, r_H the Hall factor, k_B the Boltzmann constant, and E_F the Fermi energy. The results elucidate that the initial Fermi level difference is about 0.65 eV, considering the valence band offset between the pristine and heavily doped BiCuSeO. The Fermi level difference prompts charge carriers to transfer from the doped to the pristine region; during this process, a self-built potential is set up to resist the carrier transfer due to Fermi level imbalance. An equilibrium is eventually achieved when the self-built potential is equal to the Fermi level difference. The calculated Fermi level difference is consistent with the idea proposed in Figure 1. After carrier redistribution, the carrier concentration n_1 is calculated to be about 1.02×10^{20} cm^{-3} (100 times larger than the pristine value) in the undoped BiCuSeO region, while n_2 of about 4.9×10^{21} cm^{-3} (only 2% of the original value) is left in the heavily doped $Bi_{0.75}Ba_{0.25}CuSeO$ region. Strictly speaking, the carrier mobilities should also change during carrier redistribution, but actually, the contribution due to the slight change in the carrier motilities can be safely neglected compared with that due to the change in the carrier concentrations. Combining the above parameters, the effective electrical conductivity (σ_{eff}) can be calculated as 580 S cm^{-1} in the modulation doped $Bi_{0.875}Ba_{0.125}CuSeO$, with less than 10% error compared with the experimental value (640 S cm^{-1}). This slight discrepancy between the calculated and experimental results might be from the Ba-rich segregations at the heterogeneous boundaries (discussed later) serving as an additional carrier reservoir and further promoting the charge redistribution, which is similar to the observation of extra charge carriers provided by the nanoscale metallic particles.[32,33]

The MD has a negligible effect on the Seebeck coefficient, as shown in Figure 4b. The positive Seebeck coefficient indicates a p-type electrical transport behavior. The Seebeck coefficient values of pristine BiCuSeO are large, from +353 μV K^{-1} at 300 K to +420 μV K^{-1} at 923 K, and decrease with increasing Ba doping fraction, down to +50 μV K^{-1} at 300 K and +150 μV K^{-1} at 923 K for the $Bi_{0.75}Ba_{0.25}CuSeO$ sample, which is consistent with the increased carrier concentration. The modulation doped $Bi_{0.875}Ba_{0.125}CuSeO$ possesses medium Seebeck coefficient values, + 81 μV K^{-1} at 300 K and +184 μV K^{-1} at 923 K, remaining on the same level as those of uniformly doped $Bi_{0.875}Ba_{0.125}CuSeO$, which is largely due to their comparable carrier concentrations.

For the modulation doped $Bi_{0.875}Ba_{0.125}CuSeO$, the improved electrical conductivity and nearly unaffected Seebeck coefficient

dx.doi.org/10.1021/ja507945h | J. Am. Chem. Soc. 2014, 136, 13902−13908

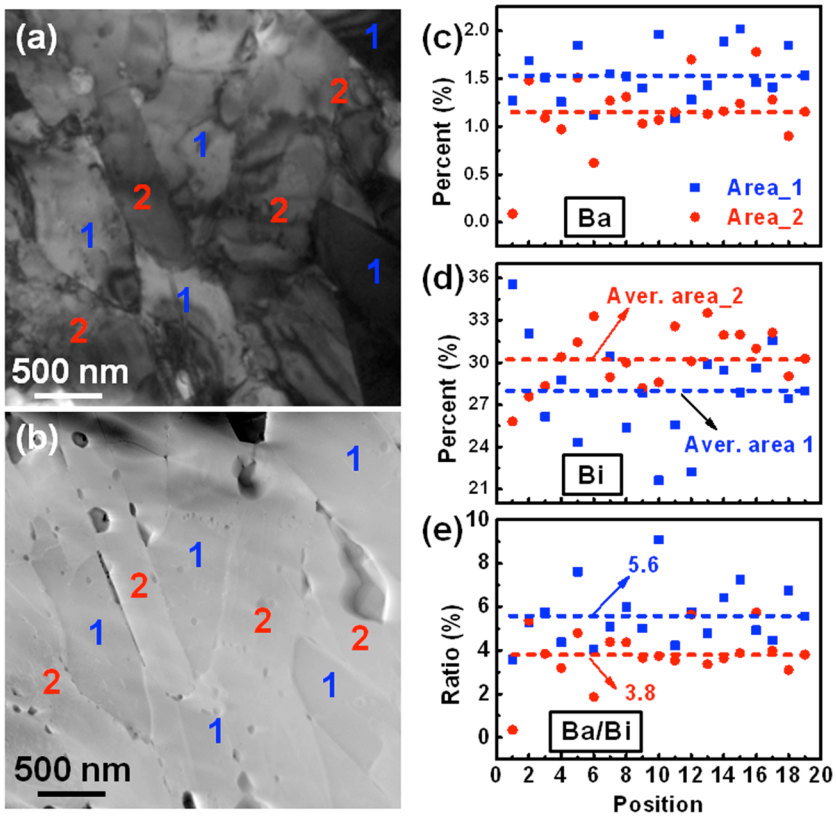

Figure 5. Microstructural features of the modulation doped sample $Bi_{0.875}Ba_{0.125}CuSeO$: (a) low-magnification BF-TEM image; (b) low-magnification HAADF image; (c,d) Ba and Bi content (EDS) in area_1 and area_2, respectively; (e) Ba/Bi content ratio in area_1 and area_2.

of the modulation doped $Bi_{0.875}Ba_{0.125}CuSeO$ lead to a broad, high power factor range from 5 μW cm^{-1} K^{-2} at 300 K to 10 μW cm^{-1} K^{-2} at 923 K; these values are even higher than those of heavily doped $Bi_{0.75}Ba_{0.25}CuSeO$ (Figure 4c). The present results elucidate that the electrical conductivity of the two-phase composite under the concept of MD exceeds that of each individual component, leading to a higher power factor.

Figure 4d shows the total thermal conductivity κ_{tot} as a function of temperature. The κ_{tot} of BiCuSeO decreases with increasing temperature, from 0.54 W m^{-1} K^{-1} at 300 K to 0.33 W m^{-1} K^{-1} at 923 K (heat capacity, thermal diffusivity data, and sample density can be found in the SI, Figure S1 and Table S1). κ_{tot} increases with increasing carrier concentration (Ba doping fractions), which is caused by the enhanced electronic heat transport contribution, but still maintains very low values over the entire measurment temperature range, e.g., 1.1 W m^{-1} K^{-1} at 300 K and 0.8 W m^{-1} K^{-1} at 923 K for heavily doped $Bi_{0.75}Ba_{0.25}CuSeO$. The lattice thermal conductivity κ_{lat} can be estimated by directly subtracting electronic thermal conductivity κ_{ele} from the κ_{tot}. κ_{ele} is proportional to the electrical conductivity σ through the Wiedemann–Franz relation, $\kappa_{ele} = L\sigma T$, where L is the Lorenz number, which is extracted on the basis of fitting the respective Seebeck coefficient values that can be used to estimate the reduced η[31,34] (see Figure S1). Lattice thermal conductivity κ_{lat} shows a decreasing trend with increasing temperature (Figure 4e). In the BiCuSeO system, the κ_{lat} is presumably reduced by point defect scattering through Ba doping based on the Callaway model,[30,35,36] where the mass and strain field fluctuations between the impurity atoms and the host lattice account for the enhanced scattering.[35,36] Indeed, a clear trend can be readily seen where the lattice thermal conductivity κ_{lat} decreases with increasing Ba doping fraction, especially in the high temperature range. Namely, the lattice thermal conductivity κ_{lat} at 923 K decreases from 0.32 W m^{-1} K^{-1} for undoped BiCuSeO to 0.22 W m^{-1} K^{-1} for the heavily doped $Bi_{0.75}Ba_{0.25}CuSeO$ sample. Interestingly, the modulation doped $Bi_{0.875}Ba_{0.125}CuSeO$ shows a lattice thermal conductivity similar to that of the uniformly doped sample. The Callaway model elucidates the point defect scattering in a solid solution system, originating from both the mass difference (mass fluctuations) and the size and interatomic coupling force differences (strain field fluctuations) between the impurity atom and the host lattice.[35,36]

Combining the electrical and thermal transport properties, the ZT is calculated as shown in Figure 4f. The expressly high power factor of ~10 μW cm^{-1} K^{-2} at 923 K couples with the extremely low thermal conductivity of ~0.25 W m^{-1} K^{-1} at 923 K, resulting in the maximum ZT value of ~1.4 at 923 K for the modulation doped $Bi_{0.875}Ba_{0.125}CuSeO$, a nearly 30% increase from $ZT \approx 1.1$ in the uniformly doped $Bi_{0.875}Ba_{0.125}CuSeO$.[21]

In order to better elucidate the underlying mechanisms of enhanced carrier mobility in the modulation doped sample compared with the uniformly and heavily doped ones, we investigate the microstructural features of the modulation doped sample via various TEM techniques. Rod-like grains can be clearly seen in the low-magnification bright-field TEM (BF-TEM) and high-angle annular dark-field (HAADF) images (Figure 5a,b). It is the intrinsic layered crystal structure of BiCuSeO that is responsible for these rod-like grains being slightly aligned during the uniaxial hot-pressing step. More importantly, these BF-TEM and HAADF images on the same

dx.doi.org/10.1021/ja507945h | J. Am. Chem. Soc. 2014, 136, 13902–13908

district clearly and complementarily exhibit two kinds of areas with slightly different contrasts. Considering the *Z*-contrast feature of the HAADF imaging mode, the contrast difference hints a slight composition difference between the two areas. Next, we performed energy-dispersive spectrometry (EDS) with a 1 nm electron probe to clarify this slight composition difference between these two typical areas. The statistical EDS spot analyses of Ba content, Bi content, and Ba/Bi content ratio in both area_1 and area_2 (Figure 5c,d, respectively) convincingly reflect that area_1 is Ba-rich (doped component) while area_2 is Ba-poor (undoped component). Ideally, the modulation sample should exhibit the coexistence of undoped component (zero Ba/Bi ratio) and doped component (25% Ba/Bi ratio); however, atomic diffusion is unavoidable during high-temperature sintering, with Ba atoms diffusing from doped grains to undoped grains. Therefore, the actual measured Ba/Bi ratios in area_1 and area_2 are about 3.8% and 5.6%, respectively. It is the existence of the relatively low doping grains that facilitate carrier transport, thanks to the enhanced carrier mobility. Meanwhile, Ba segregated regions can also be found in the modulation doped sample, especially at grain boundaries (see SI, Figure S2). These Ba segregated regions might play additional roles in determining the thermoelectric properties, e.g., phonon scattering centers and carrier reservoirs, and the latter can provide additional carriers to the undoped grains for transport when the material is subjected to an external thermal or voltage gradient.

CONCLUDING REMARKS

In summary, the high thermoelectric performance reflected by ZT = 1.4 at 923 K was achieved by improving carrier mobility through modulation doping in a BiCuSeO system. The modulation approach prompts the carrier redistribution between the two components and facilitates the electrical transport. The heterostructures of the modulation doped sample make the charge carriers transport preferentially in the low carrier concentration area, which increases the carrier mobility by a factor of 2 while maintaining the carrier concentration similar to that in the uniformly doped sample. The present results indicate that the BiCuSeO system is a robust candidate for medium-temperature thermoelectric applications. They also point out that modulation doping is an effective approach to improve the carrier mobility in three-dimensional BiCuSeO bulks, and it is highly possible that it could be applied to other thermoelectric systems.

ASSOCIATED CONTENT

Supporting Information

Experimental, characterization, and calculations details; temperature dependence of thermal diffusivity, heat capacity, Lorenz number, and electrical thermal conductivity for the pristine BiCuSeO, uniformly doped $Bi_{0.875}Ba_{0.125}CuSeO$, modulation doped $Bi_{0.875}Ba_{0.125}CuSeO$, and heavily doped $Bi_{0.75}Ba_{0.25}CuSeO$ (Figure S1); low-magnification HAADF image of modulation doped $Bi_{0.875}Ba_{0.125}CuSeO$ sample; and the elemental EDS mapping for Cu, Se, Ba, and Bi. This material is available free of charge via the Internet at http://pubs.acs.org.

AUTHOR INFORMATION

Corresponding Authors

peiyanling@buaa.edu.cn
he.jq@sustc.edu.cn

Author Contributions

#Y.-L.P. and H.W. contributed equally.

Notes

The authors declare no competing financial interest.

ACKNOWLEDGMENTS

This contribution was supported by NSFC under Grant No. 51202008 and Postdoctoral Science Foundation of China (2013M540037) (Y.-L.P), and partly supported by the startup of South University of Science and Technology of China from Shenzhen government and national 1000 plan for young scientists (J.Q.H).

REFERENCES

(1) Rowe, D. M. *CRC Handbook of Thermoelectrics: Macro to Nano*; CRC Press: Boca Raton, FL, 2006.
(2) Zhao, L. D.; Dravid, V. P.; Kanatzidis, M. G. *Energy Environ. Sci.* **2014**, *7*, 251.
(3) He, J.; Kanatzidis, M. G.; Dravid, V. P. *Mater. Today* **2013**, *16*, 166.
(4) Heremans, J. P.; Jovovic, V.; Toberer, E. S.; Saramat, A.; Kurosaki, K.; Charoenphakdee, A.; Yamanaka, S.; Snyder, G. J. *Science* **2008**, *321*, 554.
(5) Pei, Y.; Shi, X.; LaLonde, A.; Wang, H.; Chen, L.; Snyder, G. J. *Nature* **2011**, *473*, 66.
(6) Biswas, K.; He, J.; Blum, I. D.; Wu, C. I.; Hogan, T. P.; Seidman, D. N.; Dravid, V. P.; Kanatzidis, M. G. *Nature* **2012**, *489*, 414.
(7) Zhao, L. D.; Wu, H. J.; Hao, S. Q.; Wu, C. I.; Zhou, X. Y.; Biswas, K.; He, J. Q.; Hogan, T. P.; Uher, C.; Wolverton, C.; Dravid, V. P.; Kanatzidis, M. G. *Energy Environ. Sci.* **2013**, *6*, 3346.
(8) Zhao, L. D.; Hao, S.; Lo, S. H.; Wu, C. I.; Zhou, X.; Lee, Y.; Li, H.; Biswas, K.; Hogan, T. P.; Uher, C.; Wolverton, C.; Dravid, V. P.; Kanatzidis, M. G. *J. Am. Chem. Soc.* **2013**, *135*, 7364.
(9) Zhao, L.-D.; Lo, S.-H.; Zhang, Y.; Sun, H.; Tan, G.; Uher, C.; Wolverton, C.; Dravid, V. P.; Kanatzidis, M. G. *Nature* **2014**, *508*, 373.
(10) Nielsen, M. D.; Ozolins, V.; Heremans, J. P. *Energy Environ. Sci.* **2013**, *6*, 570.
(11) Morelli, D. T.; Jovovic, V.; Heremans, J. P. *Phys. Rev. Lett.* **2008**, *101*, No. 035901.
(12) Liu, J.; Wang, C.; Su, W.; Wang, H.; Zheng, P.; Li, J.; Zhang, J.; Mei, L. *Appl. Phys. Lett.* **2009**, *95*, No. 162110.
(13) Terasaki, I.; Sasago, Y.; Uchinokura, K. *Phys. Rev. B* **1997**, *56*, No. R12685.
(14) Van Nong, N.; Pryds, N.; Linderoth, S.; Ohtaki, M. *Adv. Mater.* **2011**, *23*, 2484.
(15) Flahaut, D.; Mihara, T.; Funahashi, R.; Nabeshima, N.; Lee, K.; Ohta, H.; Koumoto, K. *J. Appl. Phys.* **2006**, *100*, No. 084911.
(16) Bérardan, D.; Guilmeau, E.; Maignan, A.; Raveau, B. *Solid State Commun.* **2008**, *146*, 97.
(17) Zhao, L. D.; Berardan, D.; Pei, Y. L.; Byl, C.; Pinsard-Gaudart, L.; Dragoe, N. *Appl. Phys. Lett.* **2010**, *97*, No. 092118.
(18) Zhao, L. D.; He, J. Q.; Berardan, D.; Lin, Y. H.; Li, J.-F.; Nan, C. W.; Dragoe, N. *Energy Environ. Sci.* **2014**, *7*, 2900.
(19) Li, J.; Sui, J. H.; Barreteau, C.; Berardan, D.; Dragoe, N.; Cai, W.; Pei, Y. L.; Zhao, L. D. *J. Alloys Compd.* **2013**, *551*, 649.
(20) Pei, Y. L.; He, J. Q.; Li, J. F.; Li, F.; Liu, Q. J.; Pan, W.; Barreteau, C.; Berardan, D.; Dragoe, N.; Zhao, L. D. *NPG Asia Mater.* **2013**, *5*, No. e47.
(21) Li, J.; Sui, J. H.; Pei, Y. L.; Barreteau, C.; Berardan, D.; Dragoe, N.; Cai, W.; He, J. Q.; Zhao, L. D. *Energy Environ. Sci.* **2012**, *5*, 8543.
(22) Lan, J.-L.; Liu, Y.-C.; Zhan, B.; Lin, Y.-H.; Zhang, B. P.; Yuan, X.; Zhang, W. Q.; Xu, W.; Nan, C. W. *Adv. Mater.* **2013**, *25*, 5086.
(23) Liu, Y.; Zhao, L. D.; Liu, Y. C.; Lan, J. L.; Xu, W.; Li, F.; Zhang, B. P.; Berardan, D.; Dragoe, N.; Lin, Y. H.; Nan, C. W.; Li, J. F.; Zhu, H. M. *J. Am. Chem. Soc.* **2011**, *133*, 20112.
(24) Sui, J. H.; Li, J.; He, J. Q.; Pei, Y. L.; Berardan, D.; Wu, H. J.; Dragoe, N.; Cai, W.; Zhao, L. D. *Energy Environ. Sci.* **2013**, *6*, 2916.

(25) Poehler, T. O.; Abraham, D. *Appl. Phys. Lett.* **1965**, *6*, 125.
(26) Tsukazaki, A.; Akasaka, S.; Nakahara, K.; Ohno, Y.; Ohno, H.; Maryenko, D.; Ohtomo, A.; Kawasaki, M. *Nat. Mater.* **2010**, *9*, 889.
(27) Zebarjadi, M.; Joshi, G.; Zhu, G.; Yu, B.; Minnich, A.; Lan, Y.; Wang, X.; Dresselhaus, M.; Ren, Z.; Chen, G. *Nano Lett.* **2011**, *11*, 2225.
(28) Yu, B.; Zebarjadi, M.; Wang, H.; Lukas, K.; Wang, H.; Wang, D.; Opeil, C.; Dresselhaus, M.; Chen, G.; Ren, Z. *Nano Lett.* **2012**, *12*, 2077.
(29) Nan, C.-W. *Prog. Mater. Sci.* **1993**, *37*, 1.
(30) Li, S. S. *Semiconductor physical electronics*; Springer: New York, 2006.
(31) Zhao, L. D.; Lo, S. H.; He, J.; Li, H.; Biswas, K.; Androulakis, J.; Wu, C. I.; Hogan, T. P.; Chung, D. Y.; Dravid, V. P.; Kanatzidis, M. G. *J. Am. Chem. Soc.* **2011**, *133*, 20476.
(32) Zhao, H.; Pokharel, M.; Chen, S.; Liao, B.; Lukas, K.; Opeil, C.; Chen, G.; Ren, Z. F. *Nanotechnology* **2012**, *23*, No. 505402.
(33) Koirala, M.; Zhao, H.; Pokharel, M.; Chen, S.; Dahal, T.; Opeil, C.; Chen, G.; Ren, Z. F. *Appl. Phys. Lett.* **2013**, *102*, No. 213111.
(34) Kumar, G. S.; Prasad, G.; Pohl, R. O. *J. Mater. Sci.* **1993**, *8*, 4261.
(35) Callaway, J.; von Baeyer, H. C. *Phys. Rev.* **1960**, *120*, 1149.
(36) Wan, C. L.; Pan, W.; Xu, Q.; Qin, Y. X.; Wang, J. D.; Qu, Z. X.; Fang, M. H. *Phys. Rev. B* **2006**, *74*, No. 144109.